Eur. J. Mech. B/Fluids, **17**, n° 4, 615–637, 1998

Streamwise vortices in Large-Eddy simulations of mixing layers

P. COMTE *, J. H. SILVESTRINI, P. BÉGOU

ABSTRACT. – The formation of three-dimensional vortices in spatially-growing incompressible mixing layers is investigated in Large-Eddy Simulation at zero molecular viscosity, with the aid of the Filtered Structure Function subgrid-scale model proposed in Ducros *et al.* (1996, *J. Fluid Mech.*, **326**, pp. 1–36). Up to the second pairing at least, strong sensitivity to the nature of the random upstream perturbations and the spanwise size of the domain is observed. In addition to 'unequal' pairings between Kelvin-Helmholtz billows having undergone a different number of pairings and destructive 'translative-pairing-and-tearing' events, the two types of flow patterns obtained in the temporal Direct Numerical Simulations of Comte *et al.* (1992, *Phys. Fluids A*, **4**, 2761–2778), are recovered, namely, highly three-dimensional vortex lattices undergoing local or helical pairings, as in the experiments of Chandrsuda *et al.*(1978, *J. Fluid Mech.* **85**), or quasi-two-dimensional billows undergoing successive pairings while stretching streamwise vortices in between each other, as observed by Bernal and Roshko (1986, *J. Fluid Mech.*, **170**, 499–525). These streamwise vortices form *in a succession of stages involving local roll-up and pairing*, as conjectured by Lin and Corcos (1984, *J. Fluid Mech.*, **141**). Streamwise vortices are also found in a mixing layer formed within a solid-propellant rocket engine. At the wall of the outlet nozzle, they interact and possibly merge with Dean-Görtler-type vortices. © Elsevier, Paris

1. Introduction

The formation of intense three-dimensional vortices in a two-dimensional experimental or numerical facility is a challenge to human capacities at understanding and controlling nature. After more than twenty years of investigations, the most commonly accepted vision of the "canonical plane mixing layer" (i.e plane mixing layers at zero pressure gradient, as can be obtained in "clean" water or gas experimental facilities with a smooth splitter plate having a sharp trailing edge) has consisted so far of essentially spanwise Kelvin-Helmholtz billows undergoing successive quasi-two-dimensional pairings and stretching "secondary" counter-rotating streamwise vortices in between each other (Bernal and Roshko, 1986), through a mechanism proposed by Lin and Corcos (1984) and analyzed by Neu (1984). On the other hand, a completely three-dimensional vortex structure can be obtained, either "naturally" (*i.e.* in a somewhat uncontrolled manner) as in the experiment of Chandrsuda *et al.* [1] (1978), in which one of the two mixing streams is at rest, or with deterministic three-dimensional forcing as in Lasheras and Choi (1988) who used corrugated or indented splitter plates, or Nygaard and Glezer (1991; 1994) who scattered a smooth splitter plate with surface film heaters actuated by minute alternative currents. In unforced experiments, the spanwise correlation falls to 20% for a spanwise separation of about 6 times the local vorticity thickness δ (Browand and Ho, 1983), due to dislocations that strongly resemble helical pairings. We therefore agree with the following quote, from Mallier and Maslowe (1994):

Whereas pairing was long believed to be essentially a two-dimensional process, the more recent studies, as discussed by Dallard and Browand (1993), indicate that pairing is three-dimensional. This seems to be true for both laminar and turbulent mixing layers whether or not the flow is forced.

LEGI, B.P. 53, 38041 Grenoble, France. E-mail: Pierre.Comte@hmg.inpg.fr

[1] who coined the expression "helical pairing"

* Correspondence and reprints

If we nevertheless assume that three dimensionality is initially a second-order effect with respect to the straight (2D) Kelvin-Helmholtz instability, the Floquet formalism can be applied to an analytical model of Kelvin-Helmholtz vortices like the Stuart vortices. This was done by Pierrehumbert and Widnall (1982) who proposed two candidates of comparable growth rates: a couple of conjugate subharmonic modes yielding helical pairings as in Chandrsuda *et al.* (1978), and a streamwise-independent mode, referred to as *translative instability*, making the Stuart billows oscillate in phase in the spanwise direction. The growth rate of the former is maximal at zero spanwise wavenumber k_z and decreases rapidly as k_z increases. In contrast, the growth rate of the translative instability is zero in two dimensions, reaches a maximum for $k_z = (3/2)k_x$ and decreases very slowly for larger k_z. Pierrehumbert and Widnall (1982) also mentioned another, but less amplified, streamwise-independent mode causing bulging of the billows. This mode corresponds to a case of Core Dynamics Instability, a class of instabilities proposed by Schoppa *et al.* (1995) as the main cause of the *small-scale transition* first reported by Konrad (1976). In any case, since the experimental results of Bernal and Roshko (1986), the popularity of the Floquet-type secondary instability mechanisms has extended from wall-bounded flows (Orszag and Patera, 1983; Herbert, 1988) to free-shear inflectional instabilities as well, although the assumption of a steady two-dimensional primary mode of finite (but small) amplitude is more difficult to justify. However, other mechanisms have been proposed, in particular those in terms of non-linear triads (Kelly, 1967, Mallier and Maslowe, 1994) which are very appealing because of their evident analogy with the formalism of isotropic turbulence in the Fourier space: calling $\boldsymbol{p} = \pm k_a \boldsymbol{e}_x$ the most amplified Kelvin-Helmholtz mode, the most obvious $(\boldsymbol{k},\boldsymbol{p},\boldsymbol{q})$ triad that might explain helical pairings is $\boldsymbol{k} = -\boldsymbol{p}/2 \pm k_b.\boldsymbol{e}_z$ and $\boldsymbol{q} = -\boldsymbol{p}/2 \mp k_b.\boldsymbol{e}_z$, in which $k_b.\boldsymbol{e}_z$ is an arbitrary spanwise wavevector. Mallier and Maslowe (1994) found resonance [2] for inclination $\tan^{-1}(k_b/k_a) = \pm 60°$, yielding faster-than-exponential growth of the oblique waves. This mechanism is analogous to the subharmonic resonant triads that Craik (1971) proposed to explain transition in boundary layers. This is also to be the case for non-resonant models (Benney and Lin, 1960, Herbert and Morkovin, 1980), that went out of fashion to the benefit of the Floquet analysis, although they provide explanations for the formation of streaks and streamwise vortices which are, at least qualitatively, compatible with the numerical and experimental observations. Coming back to mixing layers, let us finally mention the spatial analysis by Monkewitz (1988), in which slightly oblique subharmonic modes resonate, with preferential $k_b = 0.35(\delta_i/2)^{-1}$, where $\delta_i = \Delta U/\max(d\bar{u}/dy)$ denotes the vorticity thickness of the basic hyperbolic-tangent velocity profile $\bar{u}(y)$.

In three-dimensional numerical simulations of mixing layers, it has been customary since Metcalfe *et al.* (1987) to perturb an initially laminar flow (most often of hyperbolic-tangent velocity profile) with deterministic perturbations corresponding to its most unstable eigenmodes. In our team in Grenoble, we find it complementary to use stochastic perturbations and inject small-amplitude noise, as colourless as possible, expecting to see the "natural selection" of the dominant instabilities. This was also done by Metcalfe *et al.* (1987) in a couple of cases, but the low Reynolds number of their Direct Numerical Simulations and the limited resolving power of the graphic tools available at that time tended to favor calculations yielding the simplest vortex structures, *i.e.* simulations with deterministic initial perturbations. On the other hand, spectral-eddy-viscosity SubGrid-Scale turbulence models were developed in Grenoble, thanks to which the effective Reynolds number could be increased (see the recent review of Lesieur and Métais (1996). There was thus a need for repeating the stochastically-perturbed simulations of Metcalfe *et al.* (1987) in Large-Eddy Simulation, with minimal molecular viscosity. At zero molecular viscosity, Comte *et al.* (1989) thus obtained the emergence, out of Gaussian isotropic random perturbations of energy $10^{-4}\ U^2$ (in which U denotes half the velocity difference), of two

[2] *i.e.* the same phase speed for the interacting waves, which brings the condition $c(\boldsymbol{k}) = c(\boldsymbol{p}+\boldsymbol{q}) = c(\boldsymbol{p}) + c(\boldsymbol{q})$ where $c(\boldsymbol{k}) = c(-\boldsymbol{k})$ denotes the phase speed of wavevector $\boldsymbol{k}$ given by the dispersion relation.

quasi-two-dimensional Kelvin-Helmholtz billows and a set of streamwise vortices stretched in between, all that strongly resembling the "canonical mixing layer" of Bernal et Roshko (1986). The peak values of the velocity fluctuations were in acceptable agreement with the measurements of Browand and Latigo (1979). After pairing, the spectra displayed a power-law subrange near the cut-off with a slope between -2 and $-5/3$. Taking the initial vorticity thickness δ_i as unit length, the dimensions of the domain were 14 δ_i in the streamwise direction (twice the fundamental wavelength λ_0), and 7 δ_i in the other two directions, for a resolution of $64 \times 32 \times 32$ collocation points. Repetition of this simulation in a domain twice as large in the spanwise direction (with twice as many collocation points) yielded the formation of four very distorted vortices undergoing helical pairings as they formed. Modal analysis confirmed the emergence, out of the initial noise, of modes $(1, \pm 1)$ instead of the expected fundamental mode $(2, 0)$ and its straight sub-harmonic $(1, 0)$. This simulation was repeated in Direct Numerical Simulation at initial Reynolds number $\mathrm{Re} = U\delta_i/\nu = 100$, in a $(28\ \delta_i)^3$ domain at resolution 128^3. It showed the emergence of modes $(2, \pm 1)$, yielding again an oblique vortex lattice. With a quasi-two-dimensional perturbation (energy $10^{-4}\ U^2$ in two dimensions, and $10^{-5}\ U^2$ in three dimensions), a more canonical pattern was obtained (Comte *et al.* 1992, henceforth referred to as CLL92). All these simulations have been repeated systematically by one of us (J.H.S.), in both DNS and LES with different SubGrid-Scale models, molecular Reynolds numbers and resolutions, confirming the persistence of this sensitivity to the initial perturbations for at least two pairings. Figure 1, taken from Silvestrini (1996) shows an example of a vortex lattice obtained after helical pairings. In LES with the spectral eddy-viscosity models or the filtered or selective structure function models (see, again, Lesieur and Métais, 1996, and Comte *et al.,* 1994, for a complete presentation of these), the results were found to be independent of the molecular Reynolds number as from $\mathrm{Re} = 2000$. Setting molecular viscosity to zero is a way of pushing the above SGS models to their limits. Since they assume small-scale isotropy with Kolmogorov-type power-law scalings, isotropization of all thin slender vortices could

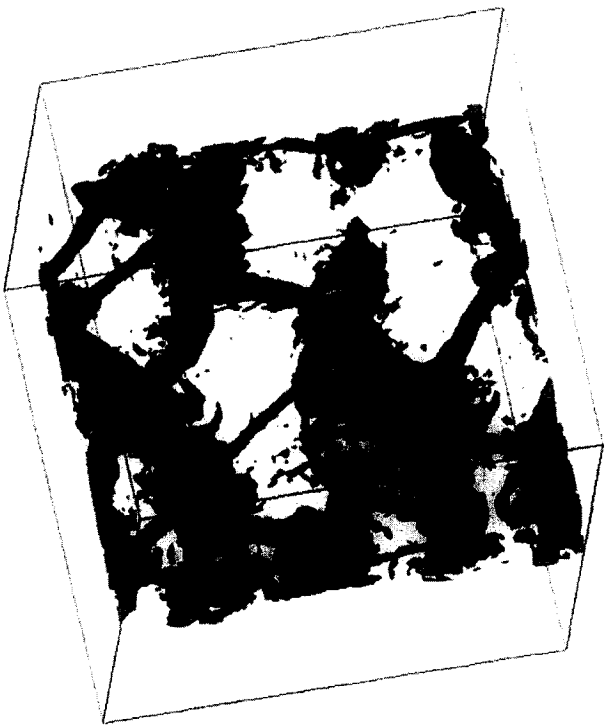

Fig. 1. – Vorticity magnitude in the LES of a temporal mixing layer forced three-dimensionally.

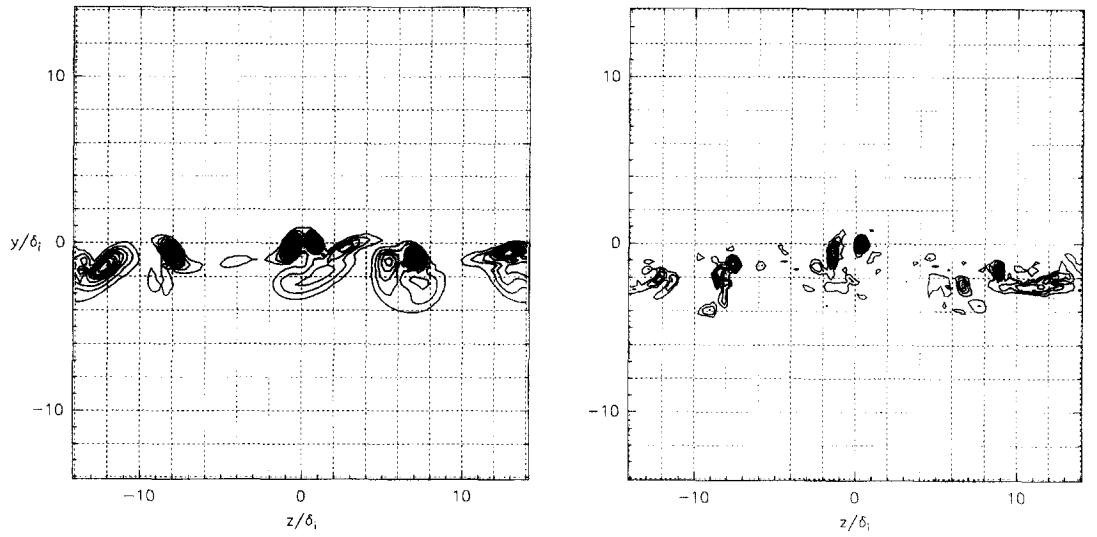

Fig. 2. – Cross-section of the vorticity magnitude showing cuts of longitudinal vortices, with full resolution on the left (DNS at Re = 100), and in LES at Re $\geq$ 2000 on the right, in fully de-aliased pseudo-spectral simulations at resolution 96^3.

have been expected. This is fortunately not the case, partly because these vortices result from large-scale instabilities that can be well resolved, and which are essentially inviscid. However, it is clear that neither the cross-section of these vortices nor the small-scale mixing properties can be correctly reproduced in such LES, whose dissipation is monitored by the resolution and other numerical considerations. To illustrate this point, Figure 2 compares cross-cuts of the vorticity field (in magnitude) across streamwise vortices in DNS and in LES with fully-dealiased pseudo-spectral methods. In the second case, the thinnest organized structures that appear as longitudinal vortices in 3D visualizations (as *Fig.* 1) are resolved over between 2 and 4 meshes, independently of the Reynolds number (at least above 2000). However, the streamwise coherence of these structures does not seem to be so dramatically influenced by the numerics, and we believe that the present extension of this approach to spatially-growing mixing layers will be more helpful than confusing. In particular, it might shed some light on certain highly controversial issues such as the degree of universality one should expect from turbulent shear flows. Indeed, as recalled in Silvestrini *et al.* (1995), the existence of a self-similar *developed* state seems to be established for all free shear flows: on these grounds, peak *rms* velocity fluctuations should be the same for all mixing layers, whatever their velocity ratio $R = (U_1 - U_2)/(U_1 + U_2)$. They should also have the same normalized spreading rate $(1/R)\ d\delta/dx$. There is nevertheless some scatter in the experimental data (the growth rates, in particular. See table below, in which δ stands for the local vorticity thickness and $U = (U_1 - U_2)/2$, as in the rest of this paper.)

On the other hand, since Brown and Roshko (1974), it has been clear that this self-similarity should concern the coherent structures as well; for example, every period doubling in the streamwise direction should be accompanied by period doubling in the spanwise direction (Bernal and Roshko, 1986). This was observed in the forced simulations of Metcalfe and Hussain (1989) and experiments of Huang and Ho (1990), but only at a statistical level, and deterministic mechanisms remain to be found out. Moreover, the vortex-structure topology seems to be much more influenced by the nature of upstream perturbations than turbulent statistics are. In other words, it is easier to control vortex patterns than turbulence level, mixing or drag.

To tackle these issues, spatially-growing simulations are required. All those we know of are low-Reynolds number Direct Numerical Simulations with deterministic upstream perturbations (Lowery and Reynolds, 1986; Buell, 1991). The main motivation of the present paper is to present analogous results in Large-Eddy Simulation

TABLE I. – Lowest and highest estimations of normalized spreading rate and *rms* velocity fluctuations among Spencer and Jones 1971 (SJ), Browand and Latigo (1979), Huang and Ho (1990), Bell and Mehta (1990). All correspond to experiments with R between 0.25 and 0.75.

	Lowest bid (Ref.)	Highest bid (Ref.)
$(1/R)\ d\delta/dx$	0.15 (BL)	0.27 (HH)
u'^2/U^2 (streamwise)	0.11 (BL)	0.14 (SJ)
v'^2/U^2 (transverse)	0.07 (BL)	0.12 (HH)
w'^2/U^2 (spanwise)	0.09 (BM)	0.11 (HH)

with stochastic upstream perturbations as in CLL92, in order to update its conclusions. This will be done in the next section.

The other motivation here is to give a proof of the practical interest of this type of simulation, in an industrial context where vortex dynamics in its three-dimensional development is of crucial importance. The case chosen is the internal gas flow within a model of solid-propellant rocket engines for the European launcher Ariane V, where shedding of coherent vortices is considered as one possible cause for the vibrations and thrust oscillations measured experimentally, the three-dimensionality of which is under debate at the moment. In section 3, results of compressible LES at finite Reynolds number will be presented briefly, showing an interesting interaction between the streamwise vortices of a mixing layer and maybe Dean-Görtler vortices, and the corresponding pressure-fluctuation spectra.

2. Incompressible mixing layers developing spatially

The numerical code used for this part of the study solves the complete Navier-Stokes and LES equations for an incompressible fluid in a parallelepipedic domain. Sixth-order compact finite-differences (Lele, 1992) are used in the longitudinal direction x, along with pseudo-spectral methods in the $y-z$ plane. Periodicity is assumed in the spanwise direction z. Sine/cosine expansions are used in the transverse direction y, enforcing free-slip boundary conditions. Non-reflective outflow boundary conditions are approximated by a multi-dimensional extension of Orlansky's (1976) discretization scheme, with limiters on the phase velocity. Finally, temporal discretization is performed by means of a low-storage 3rd order Runge-Kutta scheme, with a fractional step procedure for the pressure-gradient correction (see Gonze, 1993, for a detailed description of the algorithm). This code has recently been parallelized, by means of slice/pencil domain decomposition and transposition. The Fourier transforms are performed in parallel on $y-z$ slices. The domain is then reshaped and decomposed into streamwise "pencils", so that the linear systems brought about by the compact finite-difference scheme can be solved without communications between the processors.

The subgrid-scale model used is the *Filtered Structure Function* model proposed by Ducros *et al.*(1996) thanks to which the transition of a spatially-growing flat plate boundary layer was simulated.

For all the simulations presented in this section, the profile

$$\bar{u}(y) = \frac{U_1+U_2}{2} + \frac{U_1-U_2}{2}\ \tanh\frac{2y}{\delta_i} = U\left[\frac{1}{R} + \tanh\frac{2y}{\delta_i}\right] \tag{1}$$

is prescribed at the inlet, with $R = (U_1-U_2)/(U_1+U_2) = 0.5$.

Every timestep, Gaussian noise is generated in the inlet section $x=0$, either isotropically between modes k_y and k_z, or with ten times more energy in the modes $k_z=0$ than in the other modes. The first case corresponds approximately to the *helical case* of CLL92, and the second to their *quasi-two-dimensional* case. In both cases,

convolution by a Gaussian profile is applied to the three components, so that they have the same *r.m.s.* profile, of width δ_i and maximum value ε at $y = 0$.

In CLL92, the grid of collocation points was uniform, of spacing $\Delta = 0.2\ \delta_i$. Here, cubic meshes are still used, but with slightly less resolution, viz. $\Delta = 0.29\ \delta_i$. The parameters of all the runs presented hereafter are summarized in Table II. The first two (with initial N, for narrow domain $L_z = 14\ \delta_i$) are presented in the next section (2.1). Runs WFSFQ2D and WFSF3D can be considered as the spatially-growing LES counterparts of the *quasi-2D* and *helical* DNS of CLL92 (same L_y, L_z and forcing amplitude). They are compared in section 2.2.

TABLE II. – Recapitulative table of the simulations presented. (L_x, L_y and L_z denote the domain dimensions in the streamwise, transverse and spanwise directions, respectively. The corresponding numbers of collocation points N_x, N_y and N_z are such that all meshes are cubic of side $\Delta \approx 0.29\ \delta_i$).

RUN	ϵ	Re	$L_x/\delta_i,\ L_y/\delta_i,\ L_z/\delta_i$	N_x, N_y, N_z
NDNSQ2D	$3\ 10^{-2}$	100	140, 28, 14	480, 96, 48
NFSFQ2D	$6\ 10^{-3}$	-	112, 28, 14	384, 96, 48
WFSFQ2D	$6\ 10^{-3}$	-	112, 28, 28	384, 96, 96
WSF3D	$6\ 10^{-3}$	-	112, 28, 28	384, 96, 96

2.1. NARROW-DOMAIN SIMULATIONS

In the two-dimensional temporally-growing simulations of Lesieur *et al.* (1988) the first roll-up occurred at $t_0 = 15\ \delta_i/U$. Assuming that the local vorticity thickness δ doubles with every pairing, and that each pairing takes about 10 turn-over times δ/U (yielding temporal spreading rate $d\delta/dt = 0.1\ U$, on average over up to four pairings, to be compared with the spatial experimental values in Table I), the n-th pairing was expected at $t_n = [15 + 10\ 2^n]\ \delta_i/U$. In spatial development, this would correspond to a streamwise distance $x_n = [15 + 10\ 2^n]\ \delta_i/R$.

In the experiments of Huang and Ho (1990) for which the spatial spreading rate $(1/R)\ d\delta/dx$ is 0.27, the first roll-up occurs at $x_0 = 2\ \lambda_0/R = 14\ \delta_i/R$, the first and second pairings at $x_1 = 4\ \lambda_0/R$ and $x_2 = 8\ \lambda_0/R$, respectively. In run NDNSQ2D, the first roll-up occurs, on average, at $x_0 \approx 75\ \delta_i$ and the first pairing at $x_1 \approx 120\ \delta_i$. Each position fluctuates in time with an amplitude of about one local streamwise spacing λ between the two nearest billows, as in Huang and Ho (1990). As noticed by a referee, this certainly comes from the random nature of the upstream perturbations, but we will see, in run NFSFQ2D, complex vortex

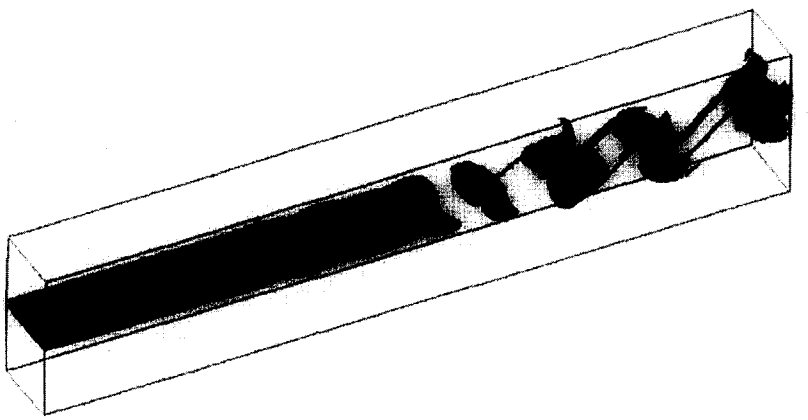

Fig. 3. – Perspective view of isovorticity surface $\|\vec{\omega}\| = \omega_i/3$ (run NDNSQ2D).

interactions likely to enhance this kind of intermittent behaviour. Coming back to run NDNSQ2D (*Fig.* 3, taken after a couple of spin-up times RL_x/U, shows the isosurface of vorticity magnitude $\|\boldsymbol{\omega}\| = \omega_i/3$, in which $\omega_i = 2U/\delta_i$ denotes the maximal vorticity magnitude brought about by the basic flow (1). The peak value of $\|\boldsymbol{\omega}\|$ recorded at this timestep is $2\omega_i$. It is reached in a streamwise vortex which connects two rolls that have already undergone one pairing. This observation applies for all the timesteps that have been looked at.

Run NFSFQ2D is a LES restart of NDNSQ2D at zero molecular viscosity. With the same upstream forcing, roll-up occurs much earlier. The forcing amplitude is then reduced to $\varepsilon = 6\ 10^{-3}$, so that the kinetic energy injected in two and three dimensions matches the respective values $10^{-4}\ U^2$ and $10^{-5}\ U^2$ of the *quasi-two dimensional* temporally-growing DNS of CLL92. In order to leave more clearance at the outlet and minimize the numerical cost, the length L_x of the domain is reduced to 112 δ_i with the same mesh size as before. As can be seen from the animated sequence in Figure 4, which shows an excerpt of the evolution of the whole vorticity-magnitude isosurface $\|\boldsymbol{\omega}\| = 2/3\ \omega_i$ seen from the side, roll-ups still occur farther upstream than in run NDNSQ2D: about $x = 40\ \delta_i$. On average, the first pairing begins at $x \approx 50\ \delta_i$ and is completed at $x \approx 70\ \delta_i$. The second begins at $x \approx 75\ \delta_i$ and is not quite finished at the outlet. As before, these positions fluctuate in time with an amplitude of the order of the local λ, that is, ≈ 8.6 and 17 δ_i for the first and second pairings respectively. Note that, as for NDNSQ2D, the most upstream measure of λ we can find is ≈ 8.6, somewhat larger than the value 7 δ_i predicted by linear stability theory independently of R (Michalke, 1964, Monkewitz and Huerre, 1982). Setting nevertheless $\lambda_0 = 7\ \delta_i$ one finds, in the terminology of Huang and Ho (1990), $x^* = Rx/\lambda_0 = 2.9$ for the first roll-up, between 3.6 and 5 for the first pairing, between 5.4 and slightly more than 8 for the second pairing. This is quite compatible with the average values found by Huang and Ho (1990), which are 4 for the first pairing and 8 for the second one.

As can be seen in Figure 4, run NFSFQ2D is visibly more turbulent than NDNSQ2D. The maximal vorticity magnitude is $\approx 4\ \omega_i$ for the whole run, and visualizations require the magnitude of all thresholds to be approximately doubled with respect to run NDNSQ2D. Figure 5 is the counterpart of Figure 3. It shows a tripling in the third quarter of the domain, followed by a regular second pairing. Figure 6 shows the streamwise vortices at the same instant. The arrows in these figures point at a value $3.6\ \omega_i$, recorded inside a streamwise vortex which wraps around the tripling and the second pairing mentioned above. The maximum-maximorum value recorded at this timestep ($\|\vec{\omega}\| = 4\ \omega_i$) lies within the second-pairing billow, and corresponds to the

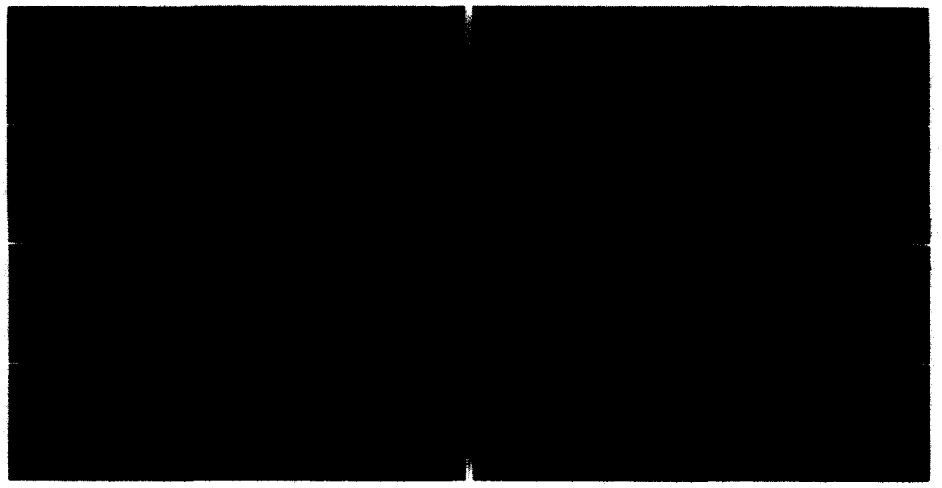

Fig. 4. – Time evolution of isovorticity surface $\|\vec{\omega}\| = 2\ \omega_i/3$ (run NFSFQD) seen from the side, to be looked at from left to right and top to bottom. The plots are labelled from (a) to (h).

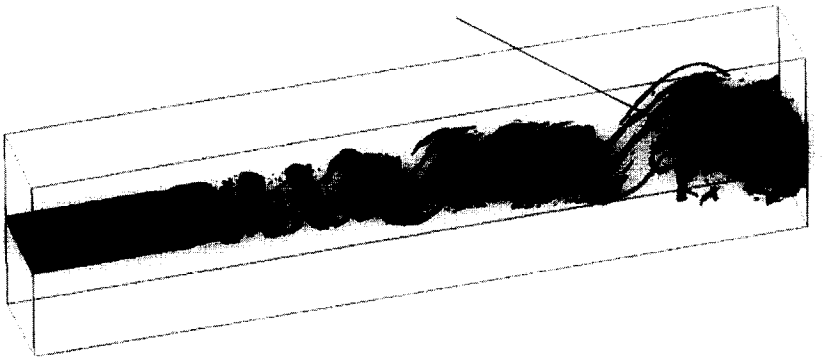

Fig. 5. – Run NFSFQ2D; isosurface $\|\omega\| = 2/3\omega_i$.

Fig. 6. – Run FSFQ2D; iso-surfaces $\omega_x = 0.5\omega_i$ (black) and $\omega_x = -0.5\omega_i$ (light grey). Portion $x < 40\ \delta_i$ of domain not shown.

remains of a streamwise vortex embedded inside it. This suggests that the streamwise vortices trapped during pairings keep their organization and keep on being stretched. Upstream of this second pairing, the streamwise vortices are more numerous but less intense. Figure 7 indeed suggests that the average spanwise spacing and diameter of the streamwise vortices double every time the spanwise billows pair.

Let us now look in perspective at the same time sequence as in Figure 4, which shows interesting and maybe new vortex interactions. Colour will be used to make out the sense of rotation of the streamwise vortices. Before looking at vorticity, it is necessary to extract and comment on the dynamics of the largest and the most intense vortices. This is the purpose of Plate 1, which shows the time evolution of the isosurface of $\langle p(t) \rangle - p_{rms}(t)$, the angle brackets corresponding to space averaging over the whole domain at time t. This low-pressure isosurface is coloured by $\omega_{3D} = (\omega_x/|\omega_x|).\sqrt{\omega_x^2 + \omega_y^2}$. The colourmap is such that two-dimensional regions, where ω_{3D} is nearly zero, appear in green, three-dimensional regions where $\omega_{3D} \geq \omega_i/2$ in red, and those where $\omega_{3D} \leq -\omega_i/2$ in blue. The domain is duplicated in the spanwise direction. As in Figure 4, the time evolution proceeds from left to right then top to bottom, and the different instants are denoted (a),..., (h). In plot (a) (top left), one can make out two quasi-two-dimensional large billows, that have already undergone pairings, the most upstream being caught up on by a very distorted thinner billow, which has not undergone any pairing yet. This is the beginning of what can be called an 'unequal' pairing, between two vortices that have undergone a different number of pairings, and does not quite correspond to the usual definition of a tripling, in which three distinct vortices are involved. Thinner 'streamwise' vortices (with, in fact, up to about 45° inclination in a horizontal plane) wrap around the billows under 'unequal pairing', and seem to originate from the 'inflection

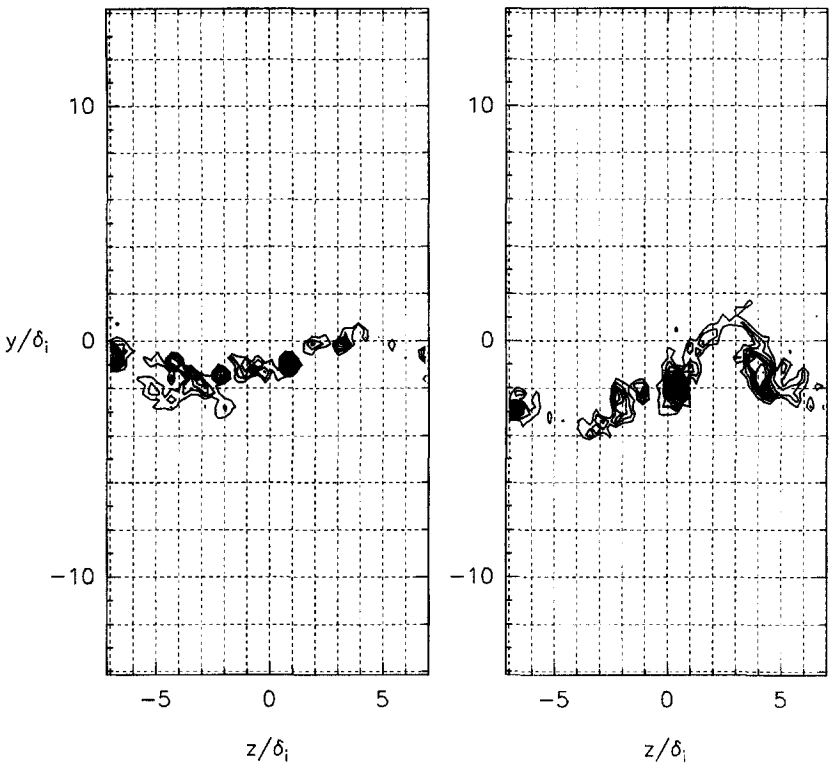

Fig. 7. – Cross-section of the vorticity magnitude showing cuts of longitudinal vortices in run NFSFQ2D, before pairing at $x = 58\ \delta_i$ (left), and after, at $x = 88\ \delta_i$.

points' of the distorted one (*i.e.* the positions where its global curvature switches signs). The other billows upstream are 'unpaired' Kelvin-Helmholtz vortices, strongly distorted three-dimensionally, approximately in phase, which is reminiscent of the translative instability investigated at infinitesimal amplitude by Pierrehumbert and Widnall (1982). It is thus tempting to claim that these vortices result from the non-linear evolution of a mode of translative instability that emerges out of the random perturbations injected at the upstream boundary.

Plot (b) (top right) is taken after the evacuation of the most downstream billow visible in plot (a). The most upstream fundamental billow about to form in plot (a) comes second in plot (b), preceded by a new Kelvin-Helmholtz vortex, much less distorted than its counterpart in plot (a). With these landmarks, the evolution of all other vortices can be easily followed from one plot to another: the large bulging billow near the outlet in plot (b) is the result of the 'unequal' pairing mentioned above. Upstream of it, the broken oblique tubes correspond to the already broken structure visible in plot (a) upstream of the 'unequal pairing'. This structure corresponds to a dying 'unpaired' Kelvin-Helmholtz vortex caught in the strain field of two adjacent pairings of larger vortices (see corresponding plot in Figure 4). An apparently regular pairing between fundamental Kelvin-Helmholtz vortices, strongly distorted in phase, is visible farther upstream. During their rotation around each other, as they close up, their planar in-phase arrangement becomes approximately symetric with respect to their common axis of rotation, yielding temporarily a braid of two merging twisted entwined vortices very similar to the result of a helical pairing as defined in Chandrsuda *et al.* (1978). Nevertheless, it is not at all evident that the helical mode of Pierrehumbert and Widnall (1982) is at work in this case. With the terminology of secondary instability, we would rather interpret this as the result of a straight (*i.e.* two dimensional) sub-harmonic mode acting on a developed state of translative instability, and therefore be tempted to call it 'translative pairing'.

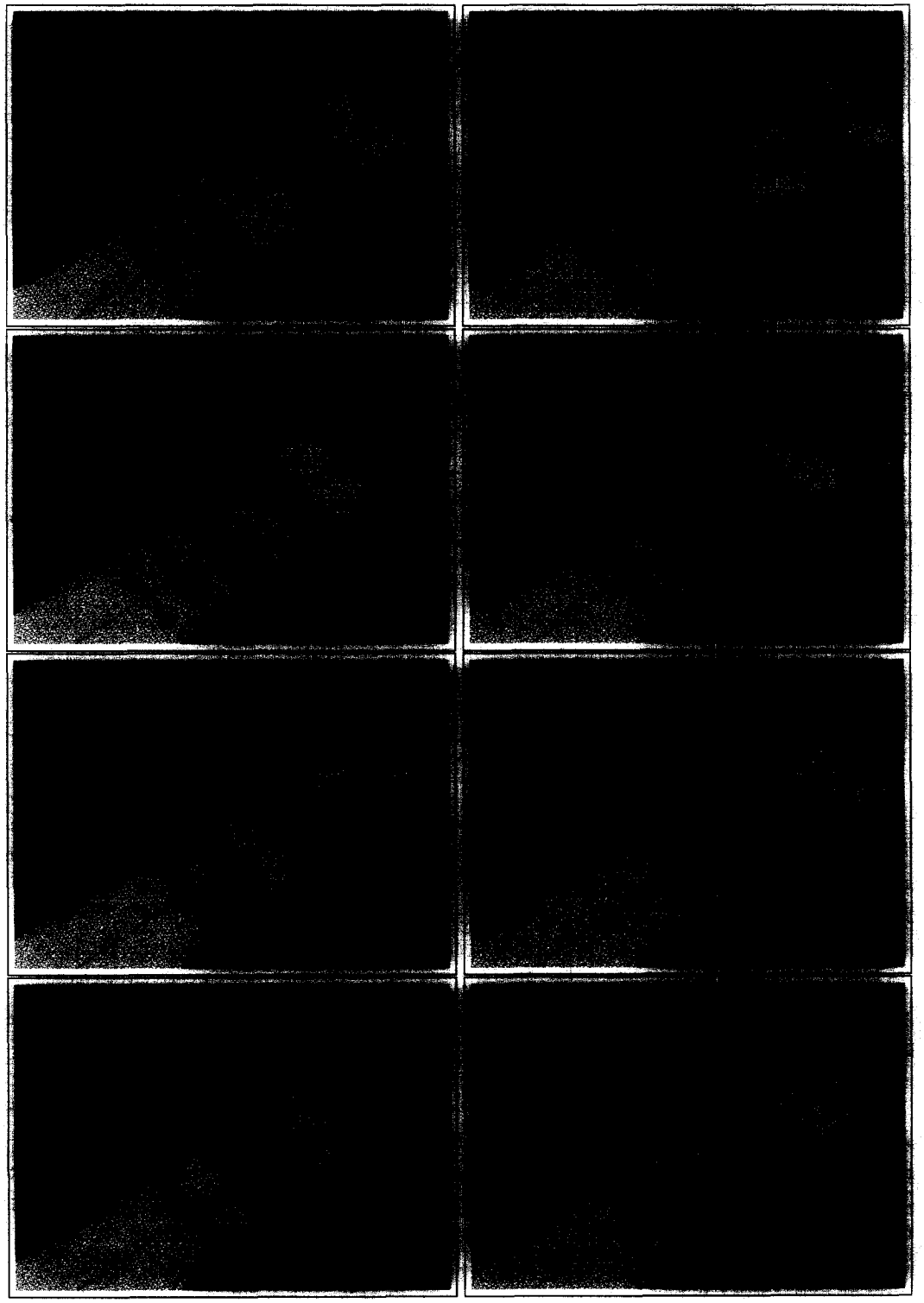

Plate 1. – Time evolution of the most intense vortices (run NFSFQ2D, domain duplicated in spanwise direction). Isosurfaces $\langle p(t)\rangle - p_{rms}(t)$ coloured by $\omega_{3D} = (\omega_x/|\omega_x|).\sqrt{\omega_x^2 + \omega_y^2}$. Zero corresponds to green, values larger than $0.6\ \omega_i$ to red and values smaller than $-0.6\ \omega_i$ to blue.

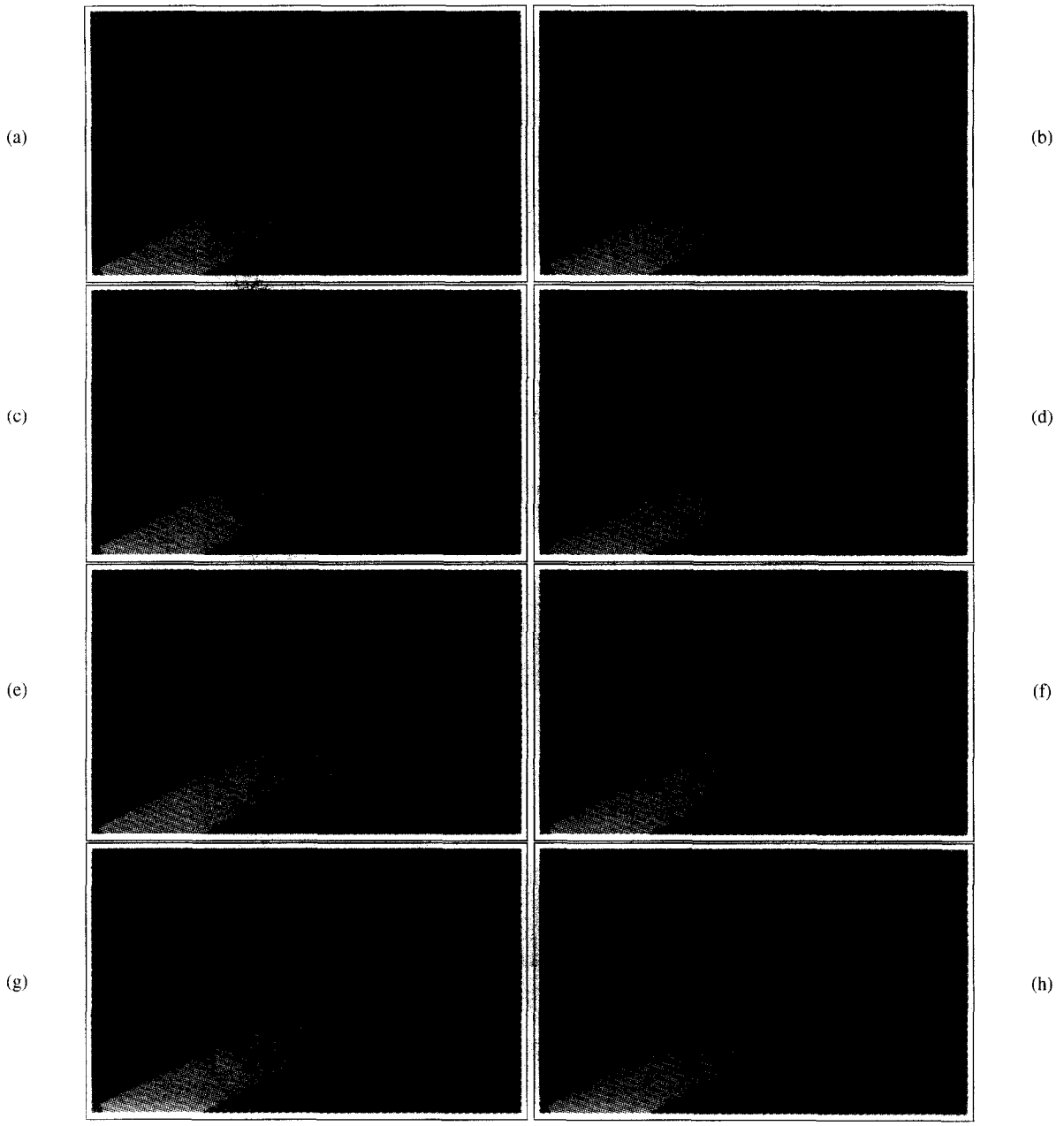

Plate 2. – Time evolution of the weaker vortices (run NFSFQ2D, domain duplicated in spanwise direction). Isosurfaces $\omega_y = 0.4\ \omega_i$ (in green and light blue to show the domain duplication), and $\omega_{3D} = \pm 0.6\ \omega_i$, the positive values in red, the negative in dark blue.

However, plots (c) and (d) (second row in Plate 1) show that the result of this interaction is unstable and boils down into a tearing event, for which an appropriate denomination will be iteratively proposed. Step-by-step inspection of intermediate images between (c) and (d) (available on e-mail request to the first author) show that the highly three-dimensional vortex lattice in red and blue in plot (d) results from the disruption of one of the vortices involved in the above tentative 'translative pairing'. The other one 're-two-dimensionalizes' (plot d), and is eventually shredded by the vortex lattice (plot e), thus contributing to the intense 'genuinely streamwise' vortices near the outlet. Note also the hairpin vortices visible immediately upstream, which reach

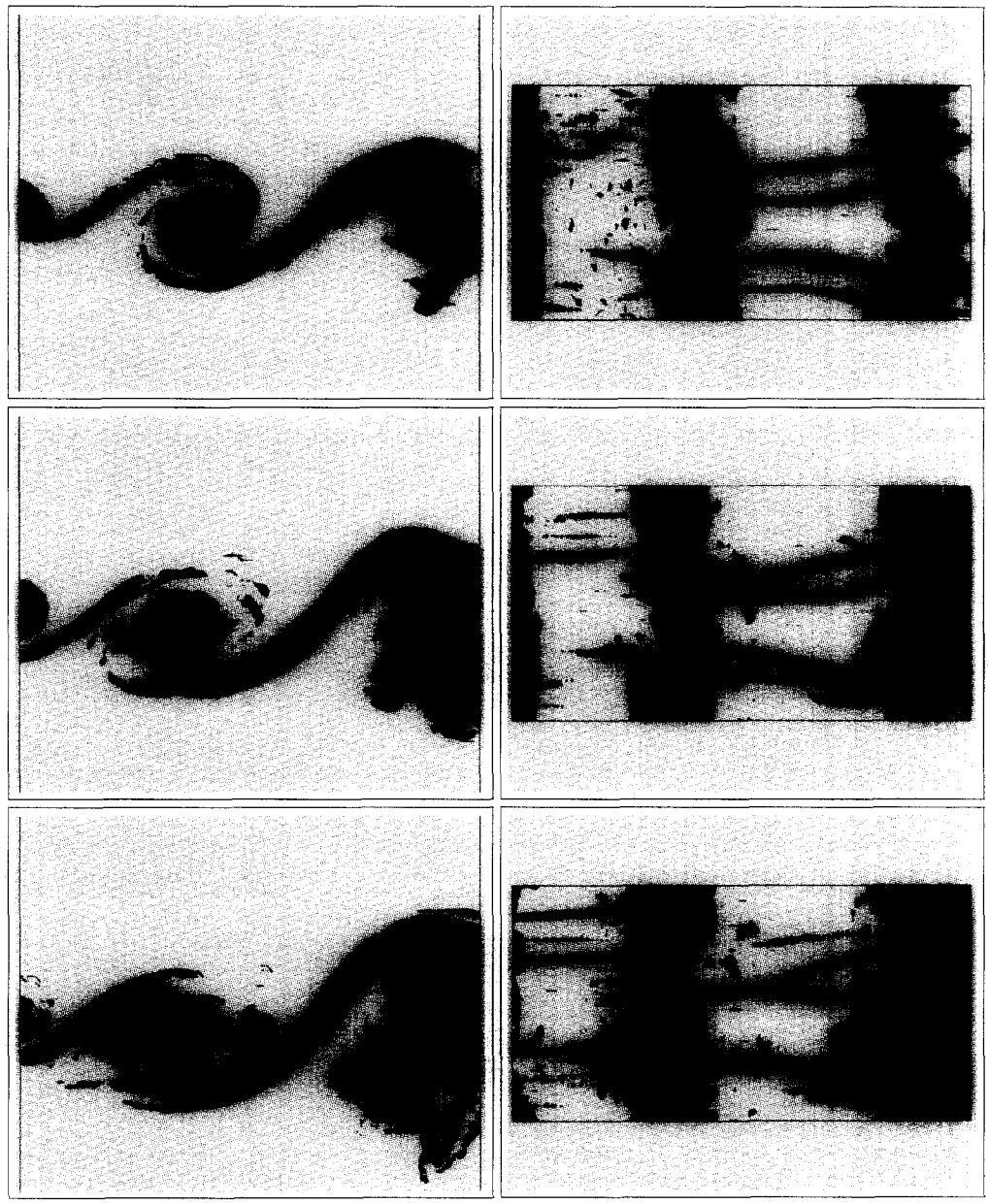

Plate 3. – Close ups of Plate 2 at times (e), (f) and (g), in top, middle and bottom rows, respectively, seen from the side in the left-hand column and from the top in the right-hand column.

the outlet in plot (f). Looking again at Plate 1 from (b) to (f), we can see that a similar fate strikes the two vortices upstream of those involved in the above 'explosive translative interaction', although the intermediate stage with a quasi-two-dimensional left in the middle of a highly three-dimensional lattice is not observed. After evacuation of these two explosive events, the flows remains calmer and the vortices more two-dimensional, sometimes slightly bulging as in plot (g), until the next explosion.

Another interesting interaction, between streamwise vortices this time, is visible on the same time sequence, when isosurfaces of different vorticity components are looked at: Plate 2 shows, at the same instants as in

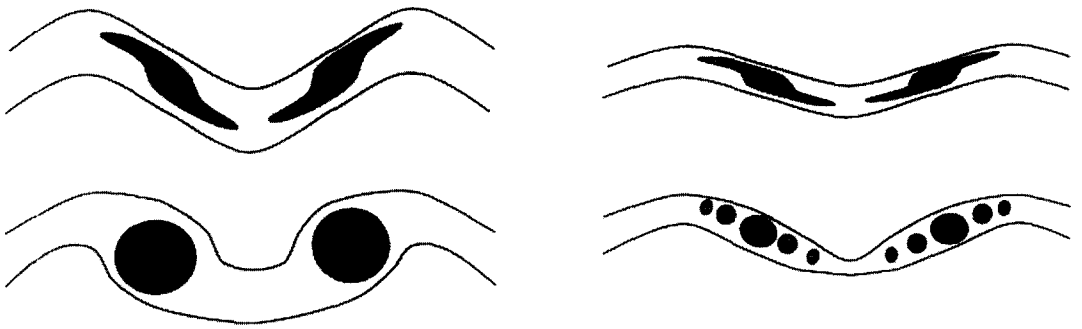

Fig. 8. – Sketch of the single-stage (left column) and multiple-stage (right column) roll-up of streamwise vortices, as conjectured by Lin and Corcos (1984). Time evolution from top to bottom in both cases.

Figure 4 and Plate 1, the isosurfaces $\omega_y = 0.4\ \omega_i$ (in green and light blue to remind one of the domain duplication), and $\omega_{3D} = \pm 0.6\ \omega_i$, the positive values in red, the negative in dark blue. In contrast with Plate 1, a large number of streamwise vortices is visible at all timesteps. Instead of a single vortex tube going back and forth in between the rollers, as conjectured by Bernal and Roshko (1986), one can see series of co-rotating streamwise vortices which converge and merge, as visible in particular in plots (e), (f) and (g), immediately upstream of the violent events reported above. Close ups from the side and the top following this region are provided in Plate 3, showing the same quantities with the same thresholds as in Plate 2, without spanwise duplication of the domain. Two braid regions are shown in Plate 3: in the leftmost third of all plots in Plate 3, the three-dimensional vorticity ω_{3D} organizes itself into streamwise structures that we claim to be vortices, although they are for the moment too weak to appear in low-pressure visualizations such as Plate 1. Stronger vortices are visible in the two rightmost thirds of the plots. At time (e) (the first row in Plate 3), these vortices appear as two pairs of nearly-parallel co-rotating structures. This does not quite fit in with the conjecture of Bernal and Roshko (1986). At time (f) (middle row), the two components of each pair converge, starting from the billows, which suggests that this secondary motion is induced by the three-dimensionality of these. The red pair (positive ω_{3D}) merges at its downstream end, and the twisting-and-pairing motion propagates upstream, relatively slowly: the merging is in fact completed just before the evacuation at the outlet, and we estimate that it takes approximately the same amount of time to complete as the pairing of the billows, although we do not have a satisfactory theoretical explanation for this yet. The two components of the blue pair cross midway and pairing propagates both upstream and downstream, although it is visible that this originates from the three-dimensionality of the downstream billow. Here again, this pairing will not be completed until the next pairing of the billows, which occurs near the outlet. Our current interpretation is that we are in the presence of a *multiple-stage* roll-up and pairing, as conjectured by Lin and Corcos (1984) and sketched in the right-hand column of Figure 8:

... In a layer where the sign of the vorticity alternates (in the direction along which strain is absent), each portion of the layer that contains vorticity of a given sign eventually contributes that vorticity to a single vortex. This may occur in a single stage if the initial layer thickness is not excessively small next to the spanwise extent of vorticity of a given sign or, otherwise, in a succession of stages involving local roll-up and pairing.

This 'multiple stage' was actually not simulated by Lin and Corcos, maybe because of the absence of a SubGrid Scale model that would permit to reduce molecular viscosity and decrease the braid thickness. Indeed, the low-Reynolds number DNS (run NDNSQ2D) showed 'single stage' roll-up of streamwise vortices. The observation of the 'multiple stage' scenario in run NLESQ2D could thus be taken as indirect proof that the effective Reynolds number of zero-molecular-viscosity LES performed with the filtered structure function model is much larger than in a DNS at the same resolution.

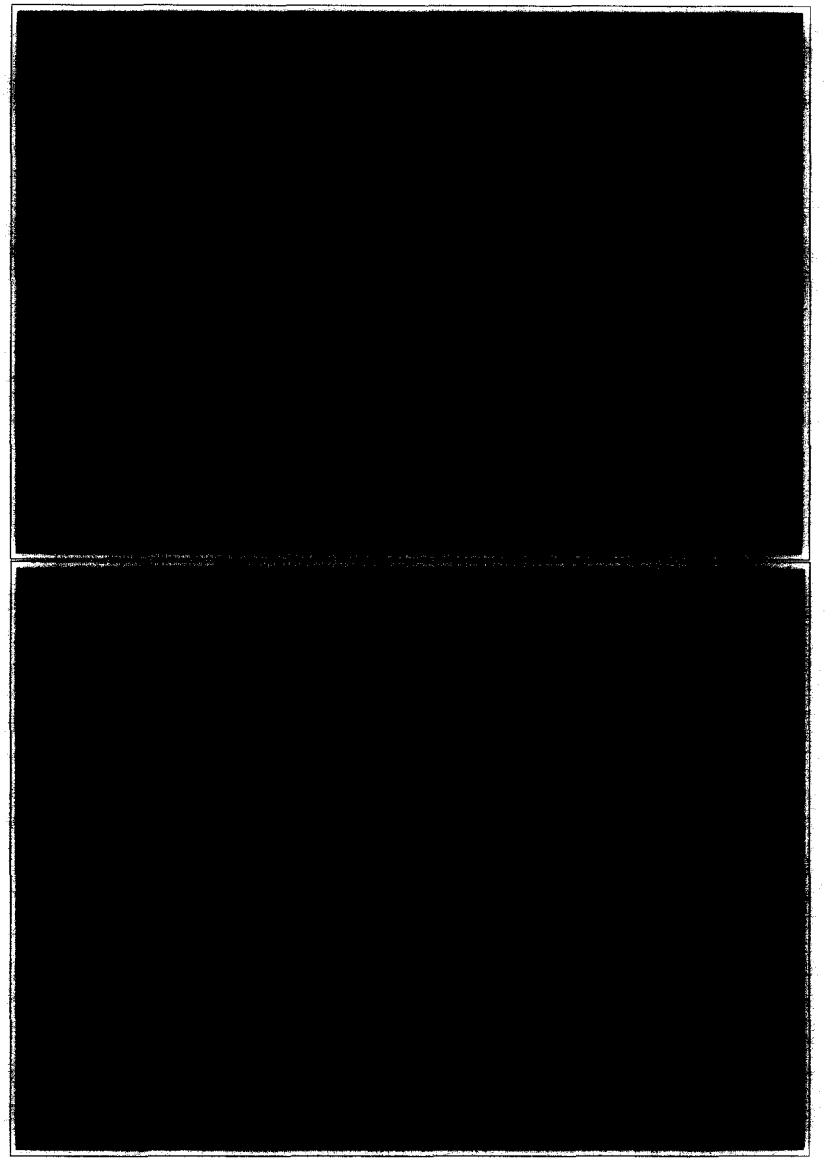

Plate 4. – a snapshot in the evolution of run WFSFQ2D. Top view: low-pressure isosurface as in plate 1. Bottom view: isosurface $\|\omega\| = 2/3\omega_i$.

2.2. WIDER-DOMAIN SIMULATIONS

Former temporal simulations (CLL92 and Silvestrini, 1996) showed an increased tendency to helical pairing in wide domains. This matches the linear secondary stability results of Pierrehumbert and Widnall (1982), although, as in CLL92, the forcing amplitudes might be too large to fulfil their hypotheses. Run WFSFQ2D is a repetition of run NFSFQ2D in a domain twice as wide, with the same upstream forcing. The initial conditions consist of a DNS velocity field at $Re = 100$, still with the same forcing. The upper view in Plate 4 shows an isosurface of the pressure field coloured according to ω_{3D}, with the same threshold and colour map as for run NFSFQ2D. Below is shown the isosurface $\|\omega\| = 2/3\ \omega_i$ at the same instant. The animation of such images shows the same intermittent trends as in run NFSFQ2D, with less translative instability and more helical pairings.

The influence of the nature of the upstream forcing is less than that of the initial forcing on temporally-growing simulations. Figures 9 and 10 are the greyscale counterpart of Plate 4 for run WFSF3D, with the same initial conditions. Although the solutions look completely decorrelated, more or less the same vortex dynamics is shown. This is confirmed in-the-mean by the animations.

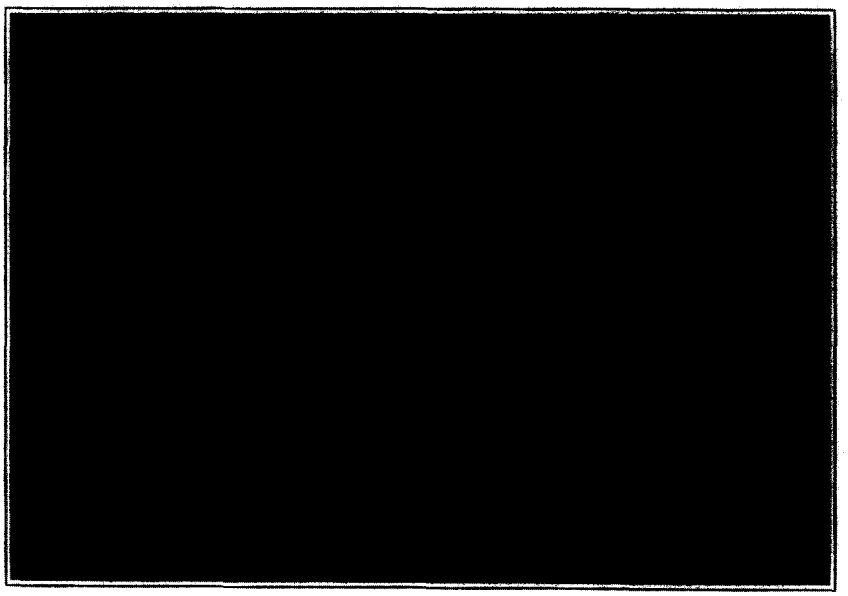

Fig. 9. – Greyscale counterpart of the top plot of Plate 4 for run WFSF3D.

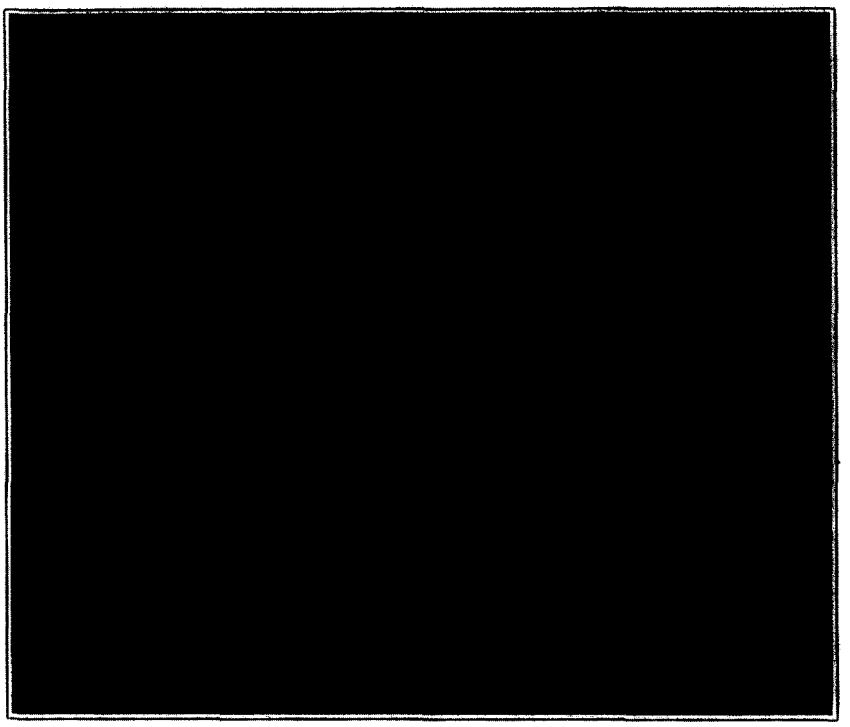

Fig. 10. – Greyscale counterpart of the bottom plot of Plate 4 for run WFSF3D.

2.3. Preliminary statistics

The following statistics are obtained from short records taken from NFSFQ2D and WFSF3D. Figure 11 shows that spreading is within the bounds of the experimental values (from $(1/R)\ d\delta/dx = 0.15$ in Browand and Latigo, 1979, to 0.27 in Huang and Ho, 1990), without the outflow boundary condition influencing it too visibly. Longer domains and time sampling are required to be conclusive about growth rates. Nevertheless WFSF3D grows slightly faster than NFSFQ2D, in the same proportion as the forced experiment of Huang and Ho (1990) does with respect to their unforced experiment. Figure 12 confirms that the domains are too short to reach self-similarity. Peak values of w'^2/U^2 are nevertheless close to those of Huang and Ho (1990): 0.09 in the unforced case and 0.15 in their forced case. The other components are overestimated, by about 25% for NFSFQ2D and 15% for WFSF3D. Note also confinement effect visible on plots of u'^2/U^2 as from $x = 81\ \delta_i$.

Energy spectra have been recorded at several locations on the centerline. Only those taken at the most downstream location are shown here (Fig. 13). More than one decade of cascade in about $f^{-2.5}$ has developed in both cases with maybe more small scales in WFSF3D than in NFSFQ2D.

3. Mixing-layer and Görtler vortices

The practical importance of the three-dimensional vortices is now briefly illustrated in the case of a model of solid-propellant rocket engine, designed by ONERA and CNES in order to explain the intermittent 'tone puffs' measured in true-scale boosters such as those of Ariane V, for which the protection of the control systems requires more than 500 kg anti-vibration protections, the largest part of which would become unnecessary if the puffs could be avoided. One of the ideas behind this joint theoretical, experimental and computational effort was that Kelvin-Helmholtz instability downstream of the propellant grains (*i.e.* blocks) and the various protruding objects (inhibitor rings), were forced by quasi-stationary acoustic modes in the combustion chamber and thus produce tone puffs, as in the early stability analysis of Flandro and Jacobs (1973). Several test cases amenable to numerical simulations, *i.e.* in simplified geometries, were designed by ONERA (see e.g. Lupoglazoff and Vuillot, 1992) in order to promote such acoustic coupling. One of these test cases, called $C1$, is planar, with a

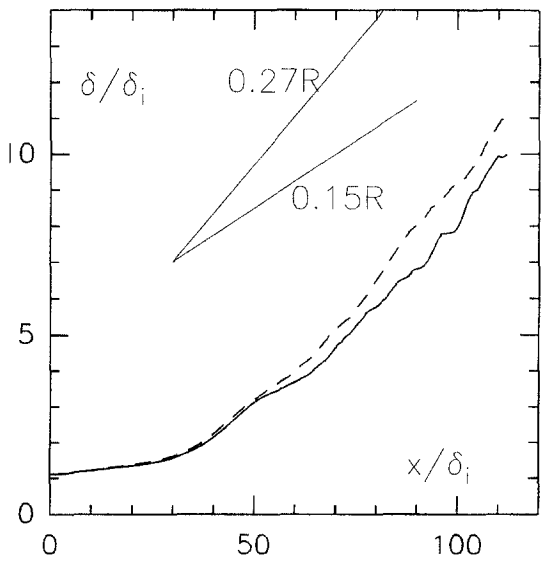

Fig. 11. – Streamwise evolution of the vorticity thickness: (—) NFSFQ2D, (- - -) WFSF3D.

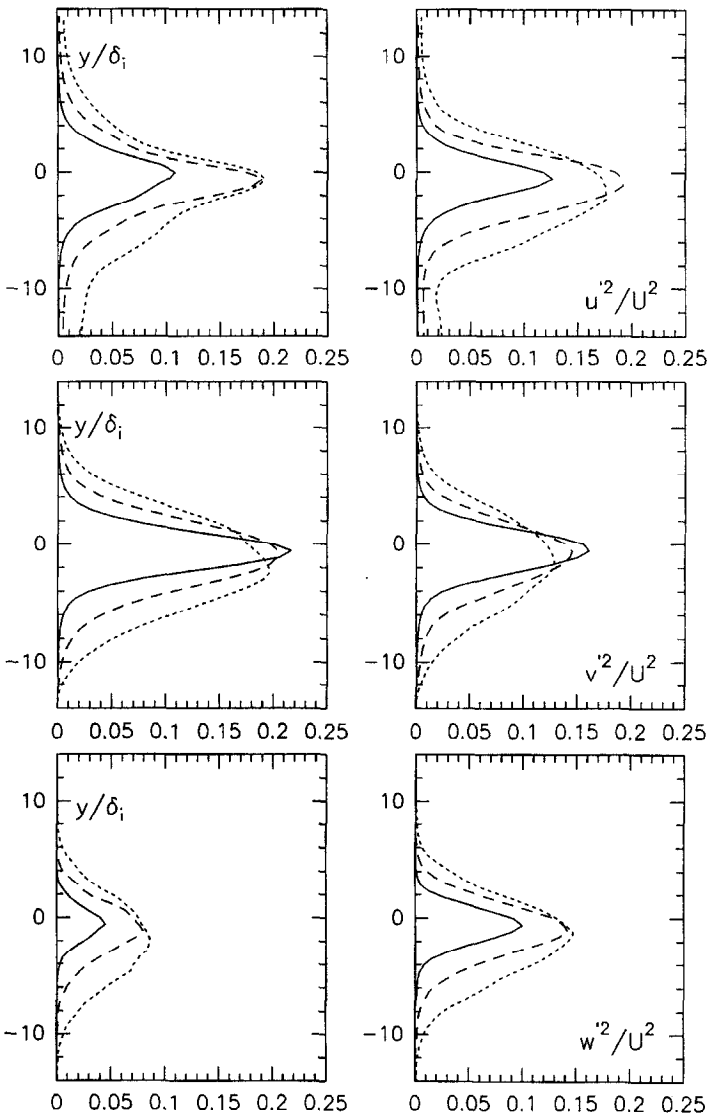

Fig. 12. – Profiles of the variance of the velocity fluctuations in run NFSFQ2D (left) and WFSF3D (right) at $x = 58\ \delta_i$ (—), $x = 81\ \delta_i$ (- - -) and $x = 104\ \delta_i$ (...).

single propellant grain of length L_{inj} having an inclined backward-facing trailing edge, a simplified nozzle and no diaphragms. The computational domain corresponds to just one half of it, with a height H corresponding to the internal radius of a projected experimental model. Combustion is modelled in a very crude manner, with prescribed mass flow-rate $\rho v_{inj} = 21.2\ \mathrm{kgm^{-2}s^{-1}}$ and flame temperature $T_f = 3387\ K$ at the surface of the propellant, whose erosion velocity is neglected. The relevant Reynolds number is the injection Reynolds number $R_{inj} = \rho v_{inj} L_{inj}/\mu(T_f)$, prescribed by ONERA at a realistic value 47000. The length of the combustion chamber (*i.e.* the distance from the front end to the sonic throat) is such that its first two quasi-stationary acoustic modes fall within the unstable range of the Kelvin-Helmholtz instability, estimated from spatial stability calculations initiated by velocity profiles measured downstream of the grain in similar situations. These profiles are close to hyperbolic tangent (see again Lupoglazoff and Vuillot, 1992), in a locally low-speed and quasi-isentropic situation. If all compressibility effects are neglected on these grounds, the Kelvin-Helmholtz

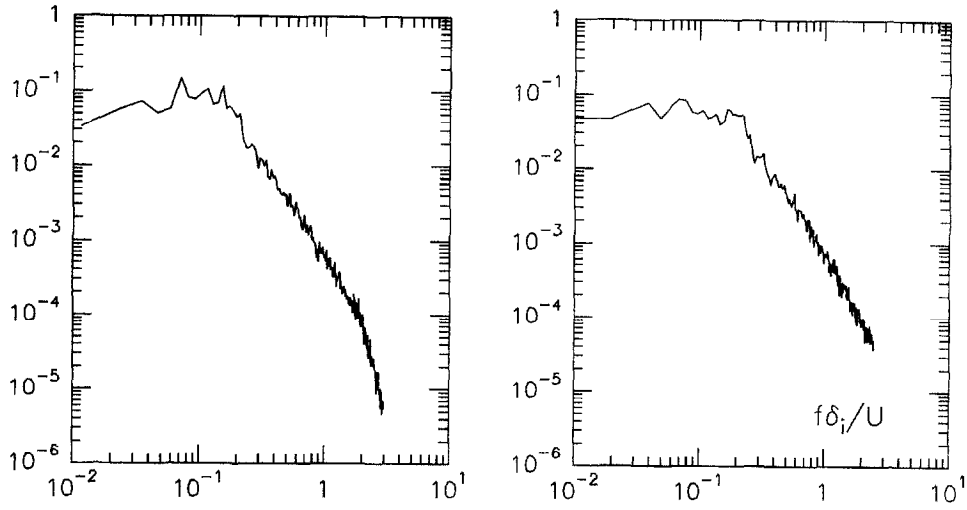

Fig. 13. – Kinetic-energy spectra at $x = 104\ \delta_i$ in NFSFQ2D (left) and WFSF3D (right).

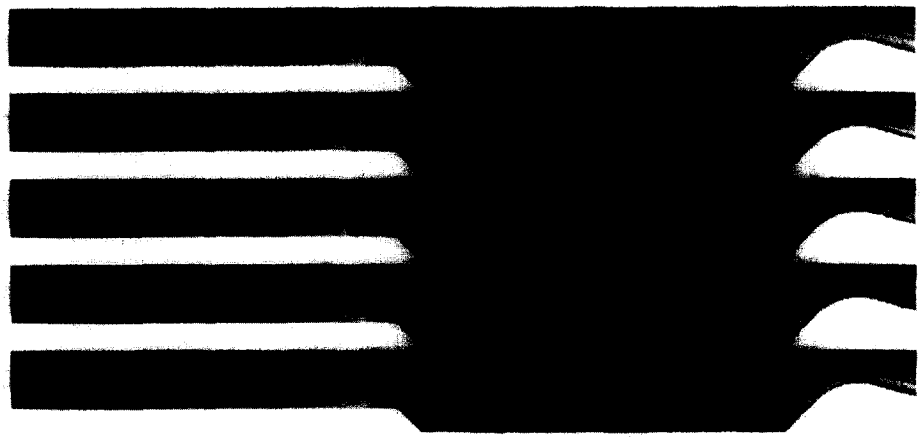

Fig. 14. – Contour maps of entropy at 5 equally spaced instants, in a low-Reynolds number 2D pseudo-DNS.

instability will be predicted as convective (Huerre and Monkewitz, 1985). All participants nevertheless found vortex shedding without any explicit forcing, which hints that acoustic coupling is really at work. The shedding frequency corresponds to that of the second longitudinal acoustic mode of the chamber. Figure 14 shows a time sequence of entropy maps over one shedding period. Temporal pressure spectra recorded in different locations confirms that the impact of the vortices on the nozzle produces pressure fluctuations that sustain the acoustic modes (the flow is subsonic up to the nozzle throat), and is thus an essential ingredient of the coupling. Note the elliptic shape of the vortices, due to confinement and compressibility effects. The simulation is performed with the aid of a (2,4) finite-difference compressible code (described in Comte *et al.*, 1995) which is a curvilinear extension of the code used in Ducros *et al.* (1996). In two dimensions, no SGS model is used, although the resolution, 318×31, is too coarse to resolve all small scales. We thus speak of 2D pseudo-direct simulation.

In three dimensions at the same Reynolds number $R_{inj} = 47000$, with the same grid as in 2D (replicated 90 times in the spanwise direction with constant space increments, for a spanwise extension πH with periodicity assumption), the filtered structure function model is used with the same code, on the grounds of a compressible

LES formalism in terms of Favre mass-weighted filtering (Comte *et al.*, 1997). Small perturbations (white noise of amplitude 10^{-4} imposed at the surface of the propellant) are required to trigger three-dimensionality. Figure 15 shows an animation of an isosurface of the magnitude of the vorticity field, with, as in Figure 14 a time interval from one plot to another equal to one fourth of the shedding period of the billows. The cross section, visible in each plot at the furthest spanwise location, is partly hidden by the isosurface, and the positions of the billows is somewhat difficult to make out. The reader is asked to accept that it is approximately given by the corresponding entropy plot in Figure 14. Indeed, in contrast with the incompressible mixing layers presented in the previous sections, the billows do not pair and their shedding remains regular, because both of the confinment and the acoustic feedback. Three-dimensionality therefore does not significantly affect the positions of the billows in this case.

Streamwise vortices are not only visible in between the large Kelvin-Helmholtz billows, but also at the wall of the nozzle, and it is not at all evident that they are all of the same origin. Indeed, the second plot of Figure 15 corresponds to an instant when the interference between the billows and the nozzle is minimal (see also the second plot in Figure 14). Surprisingly, the number of vortices that cross the sonic throat is also minimal. Moreover, these robust vortices are also visible in the other plots, independently of the unsteadiness of the billows, which suggests that they are not mixing-layer streamwise vortices. With our past experience of Dean-Görtler vortices over curved compression ramps (David, 1993, Comte *et al.*, 1994, 1995, 1997), we ascribe the quasi-steady robust vortices to a Dean-Görtler instability of the detached boundary layer which re-attaches in the convergent part of the nozzle, as checked from time-averaged streamlines. Indeed, some of these ramp-flow simulations proved to us that once they are formed, such vortices are capable of surviving sonic throats and the adverse curvature around them.

Since the resolution is clearly insufficient to resolve properly the boundary layers, in particular about the nozzle, detailed inspection of all visualizations would be somewhat premature. Two cross-cuts of the entropy field at different streamwise positions at the same instant are nevertheless shown in Figure 16, with the following cautious interpretation and discussion. In the top plot, the cross section slices a billow close to the nozzle. It shows an evident a symmetry between the top and the bottom of the billow: its top is almost two-dimensional whereas its bottom exhibits the mushroom-like shape characteristic of streamwise vortices, and is reminiscent of the Laser-Induced Fluorescence visualisations of Bernal and Roshko (1986). This asymmetry does not match the well-known conceptual model of streamwise vortices proposed in that paper, which is streamwise-periodic and therefore symetric with respect to the centerline of the mixing layer. A rapid conclusion would be to ascribe entirely our asymmetry to an external cause, *i.e.* either a smoothing effect from the no-slip boundary condition at the upper wall or a destabilizing interaction with the near-wall region, involving possibly the influence of the burning trailing edge of the propellant grain. However, in the light of the incompressible results presented in the previous sections, it seems acceptable that the intensity of the streamwise vortices increases with the downstream distance, even in the absence of pairings. When the fast stream is on top, the bottom of a billow is thus likely to be more corrugated than its top (the side views in Plate 3 might be needed to follow this argument). This effect is certainly rather weak (if not purely imaginary), otherwise it would have been noticed by Bernal and Roshko (1986).

The cross section in the bottom plot in Figure 16 cuts the mixing layer in the braid region upstream, in the vicinity of its stagnation line. It confirms the asymmetry mentioned above. Moreover, thanks to a 'colourmap' effect which was absent in figure 14, it also suggests quite strongly an interaction between mixing-layer streamwise vortices just below the stagnation line and streamwise-elongated near-wall vortices. Having checked visually that the latter correspond to the quasi-steady robust vortices, we conclude in favour of their interpretation in terms of Dean-Görtler vortices because of their large size and their relative steadiness, in contrast with the near-wall structures in compressible boundary layers obtained by Ducros *et al.* (1996) with the same numerical

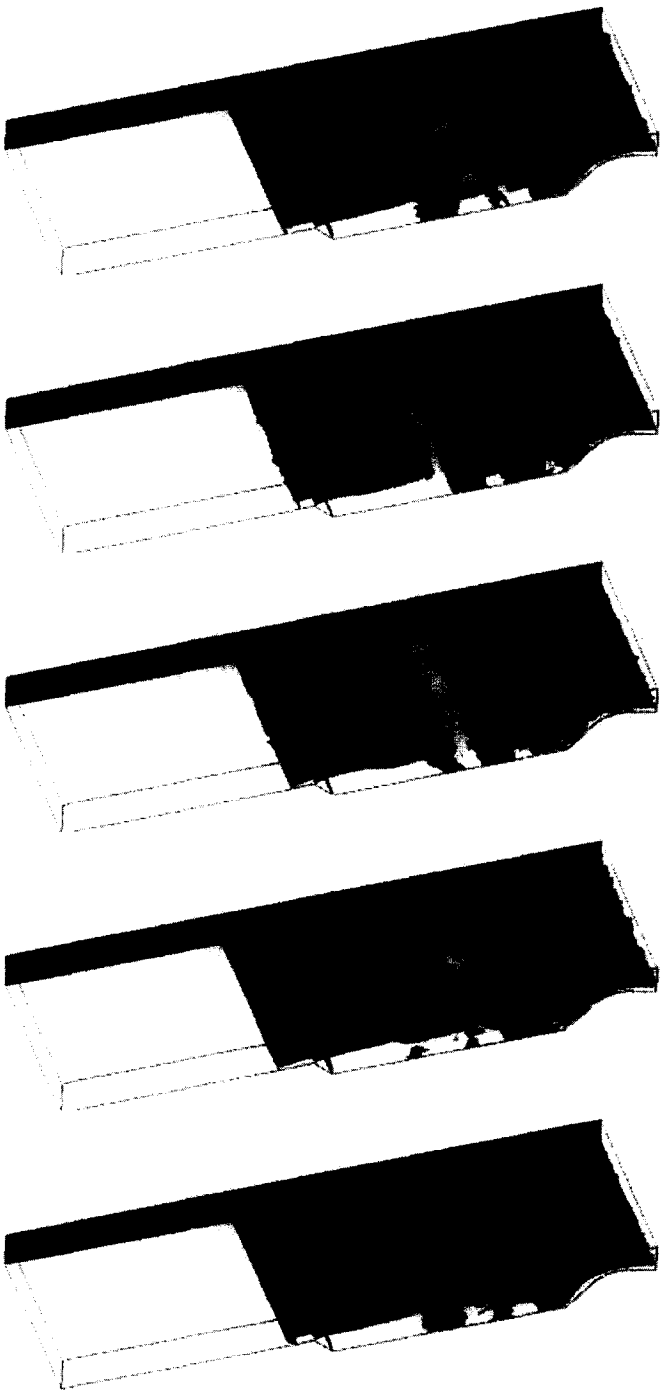

Fig. 15. – One period of the vortex shedding sequence in LES, in an "almost industrial" configuration (real time, $8ms$).

and subgrid-scale-turbulence-modeling techniques. In the light of the incompressible results presented before, pairings between these would-be Dean-Görtler vortices and the mixing-layer streamwise vortices above them cannot be excluded.

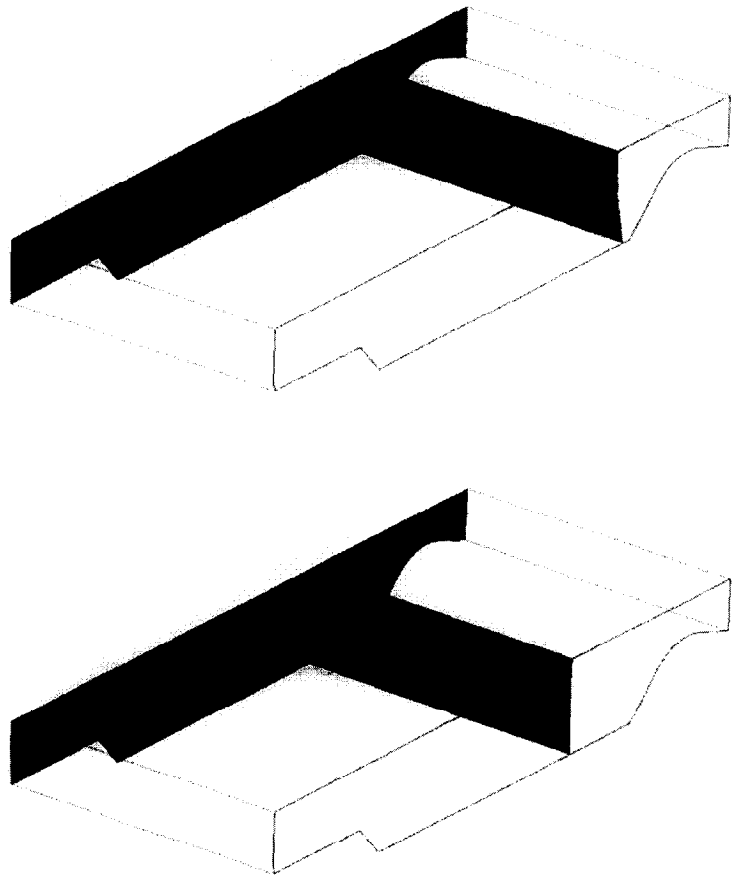

Fig. 16. – Maps of the entropy field. The top view shows a cross section of the Görtler vortices, the bottom one the streamwise vortices which connect the KH billows.

4. Conclusion

Zero-molecular viscosity Large-Eddy Simulations of spatially-growing transitional incompressible mixing layers of velocity ratio $R = 0.5$ have been performed with the aid of the Filtered Structure Function model. A level of turbulence considerably higher than in DNS at the same number of degrees of freedom has been obtained, with strong distortion of the large-scale vortices. Merging of streamwise vortices of the same sign has been observed, which is indirect proof that the effective Reynolds number of such LES is indeed large.

Intermittency of the vortex shedding is observed, with fluctuations of the roll-up and pairings positions comparable to those measured experimentally without deterministic forcing. It is partly ascribed to violent vortical events tentatively referred to as 'translative-pairing-and-tearing', during which Kelvin-Helmholtz billows distorted three-dimensionally in phase undergo two-dimensional pairing. The result is found to be unstable, yielding the disruption of the billows into a strongly three-dimensional array of thinner vortices which does not survive the next pairing.

The LES performed in a domain as wide as 4 streamwise fundamental periods of the most amplified Kelvin-Helmholtz mode exhibited far less sensitivity to the nature of the upstream forcing than temporally-growing simulations (DNS or LES) in domains of the same spanwise extension. In all cases, a strong interaction between

the so-called *primary* and *secondary* vortices was found, maximal vorticity magnitude (more than four times that of the shear prescribed at the inlet) being reached where the two are in closest contact.

Finally, a strange interaction between streamwise vortices of different origins was found in a transonic industrial application. A tentative explanation in terms of pairings between mixing-layer and Dean-Görtler streamwise vortices is proposed.

Acknowledgements. – The sequential version of the spectral/compact code for spatially-growing incompressible shear flows was written by Gonze during his PhD (1993). The CPU time on parallel or vector supercomputers was allocated free of charge by the CGCV (CEA) and IDRIS (CNRS) computing centers. The study of the vortex shedding in the boosters of Ariane V is funded by CNES/ ONERA contract $n°$ 22.492/DA/A1.CC1.

REFERENCES

BELL J., MEHTA R., 1990, Development of a two-stream mixing layer from tripped and untripped boundary layers, *AIAA J.*, **28**, 2034–2042.

BENNEY D. J., L IN C. C., 1960, On the secondary motion induced by oscillations in a shear flow. *Phys. Fluids*, **3**, 656–657.

BERNAL L. P., ROSHKO A., 1986, Streamwise vortex structure in plane mixing layer. *J. Fluid Mech.*, **170**, 499–525.

BROWAND F. K., HO C. M., 1983, The mixing layer: an example of quasi two-dimensional turbulence, Special issue on two-dimensional turbulence, *J. Theo. and Appl. Mech.*, R. Moreau ed., 99–120.

BROWAND F., LATIGO B. A., 1979, Growth of the two-dimensional mixing layer from a turbulent and non-turbulent boundary layer, *Phys. Fluids*, **22**, 1011–1019.

BROWN G., ROSHKO A., 1974, On density effects and large structure in turbulent mixing layers, *J. Fluid Mech.*, **64**, 775–816.

BUELL J., 1991, A hybrid numerical model for three-dimensional spatially-developing free-shear layers, *J. Comp. Phys.*, **95** , 313–338.

CHANDRSUDA C., MEHTA R. D., WEIR A. D., BRADSHAW P., 1978, Effect of free-stream turbulence on large structure in turbulent mixing layers, *J. Fluid Mech.*, **85**, 693–704.

COMTE P., LESIEUR M., FOUILLET Y., 1989, Coherent structures of mixing layers in large-eddy simulation, In: *Topological Fluid Dynamics*, H.K. Moffatt, A. Tsinober (eds.). Cambridge University Press, 649–658.

COMTE P., LESIEUR M., LAMBALLAIS E., 1992, Small-scale stirring of vorticity and a passive scalar in a 3D temporal mixing layer, *Phys. Fluids A*, **4**, 2761–2778.

COMTE P., DUCROS F., SILVESTRINI J. H., DAVID E., LAMBALLAIS E., MÉTAIS O., LESIEUR M., 1994, Simulation des grandes échelles d'écoulements transitionnels, 74th AGARD Fluid Dynamics Panel Meeting, Crete, p. 14.

COMTE P., SILVESTRINI J. H., LAMBALLAIS E., 1995, A straightforward 3D multiblock unsteady Navier-Stokes solver for direct and large-eddy simulations of transitional and turbulent compressible flows, 77th AGARD Fluid Dynamics Panel Symposium *Progress and Challenges in CFD methods and algorithms*, Seville, 2-5 Oct.

COMTE P., DAVID E., 1995 Large-Eddy Simulation of Görtler vortices in a Curved Compression Ramp. In *Experimentation, Modelling and Computation in Flow, Turbulence and Combustion*, Désidéri J.A., Chetverushkin B.N., Kuznetsov Y.A., Périaux J. & Stoufflet B., eds., John Wiley & Sons, pp. 45–61.

COMTE P., DAVID E., LESIEUR M., 1997, Un formalisme pour la simulation des grandes échelles d'écoulements compressibles, Preprint LEGI, for submission to C.R. Acad. Sci. Paris.

CRAIK A. D. D., 1971, Nonlinear resonant instability in boundary layers. *J. Fluid Mech.*, **50**, 393–413.

DALLARD T., BROWAND F. K., 1993, The growth of large scales at defect sites in the plane mixing layer, *J. Fluid Mech.*, **247**, 339–368.

DAVID E., 1993, Modélisation des écoulements compressibles et hypersoniques : une approche instationnaire", Doctorat de l'Institut National Polytechnique de Grenoble.

DUCROS F., COMTE, P. LESIEUR M., 1996, Large-eddy simulation of transition to turbulence in a boundary-layer developing spatially over a flat plate, *J. Fluid Mech.*, **326**, 1–36.

FLANDRO G. A., JACOBS H. R., 1973, Vortex generated sound in cavities, AAIA Paper 73-1014, Seattle, Wa, USA, October 1973.

GONZE M. A., 1993, Simulation numérique des sillages en transition à la turbulence, *Thèse* de l'Institut National Polytechnique de Grenoble.

HERBERT T., MORKOVIN M., 1980, Dialogue on bridging some gaps in stability and transition research. In *Laminar-Turbulent Transition*, ed. R. Eppler, H. Fasel, 47–72, Springer Verlag, Berlin.

HERBERT T., 1988, Secondary instability of boundary layers. *Ann. Rev. Fluid Mech.*, **20**, 487–526.

HUANG L., HO C. M., 1990, Small scale transition in a plane mixing layer, *J. Fluid Mech.*, **210**, 475–500.

HUERRE P., MONKEWITZ P. A., 1985, Absolute and convective instabilities in mixing layers. *J. Fluid Mech.*, **159**, 151–168.

KELLY R. E., 1967, On the stability of an inviscid shear layer which is periodic in space and time. *J. Fluid Mech.*, **27**, 657–689.

KONRAD J. H., 1976, An experimental investigation of mixing in two-dimensional turbulent shear flows with applications to diffusion-limited chemical reactions. Ph.D. Thesis, California Institute of Technology.

LASHERAS J., CHOI H., 1988, Three-dimensional instability of a plane free shear layer: an experimental study of the formation and evolution of streamwise vortices, *J. Fluid Mech.*, **189**, 53–86.

LELE S. K., 1992, Compact finite difference schemes with spectral-like resolution. *J. Comp. Phys.* , **103**, 16–42.

LESIEUR M., MÉTAIS O., 1996, New trends in large-eddy simulations of turbulence, *Ann. Rev. Fluid Mech.*, **28**, 45–82.

LESIEUR M., STAQUET C., LE ROI, P. COMTE P., 1988, The mixing layer and its coherence examined from the point of view of two-dimensional turbulence, *J. Fluid Mech.*, **192**, 511–534.

LIN S. J., CORCOS G. M., 1984, The mixing layer: deterministic models of a turbulent flow. Part 3. The effect of plane strain on the dynamics of streamwise vortices, *J. Fluid Mech.*, **141**, 139–178.

LOWERY P., REYNOLDS W., 1986, Numerical simulation of a spatially-growing forced, plane mixing layer. Report No. TF-26, Stanford University, California.

LUPOGLAZOFF N., VUILLOT F., 1992, Numerical simulation of vortex shedding phenomenon in 2D test case solid rocket motors. *AIAA Paper 92-0776*, 30th AIAA Aerospace Sciences Meeting Reno, USA.

MALLIER R., MASLOWE S. A., 1994, Fully coupled resonant-triad interactions in a free shear layer, *J. Fluid Mech.*, **278**, 101–121.

METCALFE R. W., HUSSAIN F., 1989, Topology of coherent strucrures and flame sheets in reacting mixing layers, in *Topological fluid Mechanics*, Moffatt, H.K. and A. Tsinober eds., Cambridge University Press, 659–668.

METCALFE R. W., ORSZAG S. A., BRACHET, M. E. MENON S., RILEY J., 1987, Secondary instability of a temporally growing mixing layer, *J. Fluid Mech.*, **184**, 207–234.

MICHALKE A., 1964, On the inviscid instability of the hyperbolic tangent velocity profile, *J. Fluid Mech.*, **19**, 543–556.

MONKEWITZ P., HUERRE P., 1982, The influence of the velocity ratio on the spatial instability of mixing layers, *Phys. Fluids*, **25**, 1137–1143.

MONKEWITZ P. A., 1988, Subharmonic resonance, pairing and schredding in the mixing layer. *J. Fluid Mech.*, **188**, 223–252.

NEU J. C., 1984, The dynamics of stretched vortices. *J. Fluid Mech.*, **143**, 253–276.

NYGAARD K., GLEZER A., 1991, Evolution of streamwise vortices and generation of small-scale motion in a plane mixing layer, *J. Fluid Mech.*, **231**, 257–301.

NYGAARD K., GLEZER A., 1994, The effect of phase variations and cross-shear on vortical structures in a plane mixing layer, *J. Fluid Mech.*, **276**, 21–59.

ORLANSKY I., 1976, A simple boundary condition for unbounded hyperbolic flows, *J. Comp. Phys.*, **21**, 251-269.

ORSZAG S. A., PATERA A. T., 1983, Secondary instability of wall-bounded shear flows, *J. Fluid Mech.*, **128**, pp. 347-385.

PIERREHUMBERT R. T., WIDNALL S. E., 1982, The two- and three-dimensional instabilities of a spatially periodic shear layer, *J. Fluid Mech.*, **114**, 59–82.

SCHOPPA W., HUSSAIN F., METCALFE R., 1995, A new mechanism of small-scale transition in a plane mixing layer: core dynamics of spanwise vortices, *J. Fluid Mech.*, **298**, 23–80.

SILVESTRINI J. H., COMTE P., LESIEUR M., 1995, DNS and LES of incompressible mixing layers developing spatially, 10th Symposium on Turbulent Shear Flows, University Park, USA, Aug. 14–16.

SILVESTRINI J., 1996, Simulation des grandes échelles des zones de mélange: application à la propulsion solide des lanceurs spatiaux. INPG PhD thesis, Grenoble, France.

SPENCER B., JONES B., 1971, Statistical investigation of pressure and velocity fields in the turbulent two-stream mixing layer, *AIAA Paper No. 71-613*, AAIA 4th Fluid and Plasma Dynamics Conference, Palo Alto, California (USA).

(Received 26 June 1997,
revised 19 February 1998,
accepted 27 February 1998)